

PAPER • OPEN ACCESS

## Research on dynamics of bouncing ball in triboelectric nanogenerator



To cite this article: Chaoming Huang *et al* 2021 *J. Micromech. Microeng.* **31** 085002

View the [article online](#) for updates and enhancements.

### You may also like

- [Formation of superscar waves in plane polygonal billiards](#)  
Eugene Bogomolny
- [Quantizing neutrino billiards: an expanded boundary integral method](#)  
Pei Yu, B Dietz and L Huang
- [Relativistic quantum scarring, spin-induced phase, and quantization in a symmetric Dirac billiard system](#)  
Zi-Yuan Li, Li-Li Ye, Rui-Hua Ni et al.

# Research on dynamics of bouncing ball in triboelectric nanogenerator

Chaoming Huang<sup>1,2</sup> , Qingtao Li<sup>2</sup>, Jie Li<sup>2</sup>, Huize Guo<sup>3</sup>, Wenhan Hao<sup>2</sup>, Kexin Sheng, Yunsheng An<sup>2</sup>, Jiayi Chen<sup>2</sup>, Xinyi Zhang<sup>2</sup> and Minyi Xu<sup>2,\*</sup> 

<sup>1</sup> College of Marine Engineering, Jimei University, Fujian 361021, People's Republic of China

<sup>2</sup> Marine Engineering College, Dalian Maritime University, Dalian 116026, People's Republic of China

<sup>3</sup> School of Department of Mechanical Engineering, The Hong Kong Polytechnic University, Hong Kong 999077, People's Republic of China

E-mail: [xuminyi@dlmu.edu.cn](mailto:xuminyi@dlmu.edu.cn)

Received 11 March 2021, revised 29 April 2021

Accepted for publication 10 June 2021

Published 25 June 2021



CrossMark

## Abstract

Bouncing ball based Triboelectric Nanogenerator (BB-TENG) can be used to harvest vibrational energy and sense signal for self-powered sensor in the non-resonant zone because of its non-spring vibration system. The energy harvesting efficiency and sensing effectiveness are significantly affected by the dynamics of the bouncing ball. However, due to the chaotic and nonlinear mechanics, the dynamics of the bouncing ball inside BB-TENG and the corresponding influencing factors have not yet been revealed, which restricts the development of high-efficiency BB-TENG. In this work a method based on dynamics simulation and test bench experiment is to be proposed and the 'Takeoff', 'Well-Contact', 'Self-Spin', and 'Rich-Contact' of the bouncing ball with the plate electrodes will be investigated. The kinetic model established based on the Automatic Dynamic Analysis of Mechanical Systems (ADAMSs) is verified through experiments to confirm the reliability of the simulation results. It is found that 'Well-Contact' of the bouncing ball makes BB-TENG harvest energy efficiently. The factors for 'Well-Contact' and their influence are investigated, and the critical frequencies for 'Well-Contact' of the bouncing ball at each vibration excitation amplitude are obtained. 'Self-Spin' of the bouncing ball produced by unbalanced excitation torque is found to increase energy harvesting, and the excitation frequency significantly determines the energy of the 'Self-Spin'. When the external excitation acceleration reaches a critical value, the 'Rich-Contact' of the bouncing ball is found, and the amount of charge transfer for BB-TENG will not increase, which is termed saturated condition. Therefore, the results of this work help improve the design and application of high-efficiency BB-TENG.

Keywords: triboelectric nanogenerator, vibration energy harvesting, bouncing ball, movement characteristics

(Some figures may appear in colour only in the online journal)

\* Author to whom any correspondence should be addressed.



Original content from this work may be used under the terms of the [Creative Commons Attribution 4.0 licence](https://creativecommons.org/licenses/by/4.0/). Any further distribution of this work must maintain attribution to the author(s) and the title of the work, journal citation and DOI.

## 1. Introduction

Various types of vibration energy are produced in our living environment at anytime and anywhere through such media as engines, bridges, vehicles, buildings, etc. If such discarded energy can be effectively utilized, additional appreciable energy will be generated to supply power for microelectronics, electronic monitoring devices and small sensors. Triboelectric nanogenerator (TENG) provides a practical way for harvesting vibration energy and transforming it into electricity.

TENG can be divided into four categories according to the operating mode: vertical contact-separation mode, contact-sliding mode, single-electrode mode, and free-standing triboelectric-layer mode [1–6]. The vertical contact-separation mode of TENG mostly use elastic elements such as springs to approach the reciprocating contact movement of the top and bottom plates, so that the energy harvesting efficiency of TENG can only be optimized near its resonance frequency band and shorten the bandwidth of energy harvesting, which limits its application. However, there is a kind of TENG cancelling the spring structure, which is represented by honeycomb structure inspired triboelectric nanogenerator (HSI-TENG) [7], hard-contact square triboelectric nanogenerator (HS-TENG) [8] and soft-contact square triboelectric nanogenerator (SS-TENG) [9]. The direct contact between the top and bottom plates is replaced by the indirect contact between the bouncing ball and the top and bottom plates. Therefore, this type of TENG has an outstanding advantage of the broadband power generation of the non-resonant system and can be used to harvest vibrational energy and sense signal for self-powered smart sensor.

Many scholars [1–5, 10] have conducted research on bouncing ball model or power generation characteristics of TENGs. The bouncing ball model was first proposed by Perutz *et al* [11], and then Luck *et al* [12] proposed the chaotic movement of the bouncing ball, and studied the chattering, locking, and chaos movements with a finite restitution. Barroso *et al* [33] modeled dynamics with a discrete map of difference equations, which reveals a rich variety of nonlinear behaviors. Smith *et al* [34] investigated the dynamics of a ball bouncing on a rough vibrating surface and the energy dissipation as a consequence of the coupling between the collision, rotation and surface friction. Due to the non-linear behavior and chaotic motion of the bouncing ball in the process of motion, many of the above motion characteristics of bouncing ball are based on ideal state assumptions, and cannot be used as a reference for the dynamic characteristics of the bouncing ball in the actual BB-TENGs. Many scholars at home and abroad have explored the power generation characteristics of TENG and the ways to optimize such characteristics. Zhang *et al* [35] studied the power generation characteristics of the liquid metal acceleration sensor by changing the material and structure. As the inventor of HSI-TENG, Xu's team [36] explored the power generation characteristics of HIS-TENG by changing the structure and working conditions; In the wind speed sensor test, the influence of different working conditions and materials on the power generation characteristics is

studied, and it is concluded that the sensor has high accuracy at a wind speed of approx.  $10 \text{ m s}^{-1}$ . Garcia *et al* [13–15] used a dynamic mechanical analyzer to study the relationship between the mechanical stimulation and the electrical response of the triboelectric nanogenerator. During the development of its impact sensor, the relationship between working conditions and power generation characteristics was discussed. Many scholars [4–6, 16–36] often discussed the power generation characteristics of TENG by changing the test conditions, structure and other variables in the development and optimization of TENG. However, few researches have been made on the dynamic characteristics of TENG regarding its power generation performance.

The power generation characteristics of BB-TENG mainly depends on the dynamics of the bouncing ball between the top and bottom plate. However, it is difficult to build up an accurate mathematic model to describe the complicate movements of the bouncing ball. And it is also hard to make effective measurements of the bouncing ball's movements in experiments. To address this need, this article proposed a method to systematically investigate movements of the bouncing ball in BB-TENG based on dynamics simulation and test bench experiment. It verified the accuracy of the parameter settings of the simulation model through the test bench. Through the visualization window of the simulation software, we obtained four key motion gestures of the bouncing ball with the plate electrodes: 'Takeoff', 'Well-Contact', 'Self-Spin' and 'Rich-Contact'. At the same time, the finite element method was used to calculate the various parameters (e.g. Speed, acceleration, displacement, etc) of the TENG model in the working process, and the reasons for the above four postures and the influence of various postures on its power generation performance were further explored. The results can help improve the design and application of high-efficiency BB-TENG for energy harvest and signal sensing.

## 2. Kinetic model

### 2.1. Dynamics equation

The bouncing ball system of the BB-TENG under investigation consists of a ball bouncing vertically on a harmonically vibrating cell. Figure 1 illustrates the bouncing ball system of the BB-TENG. The position of the cell bottom plate at time  $t$  is given by

$$S(t) = A \sin(\omega t). \quad (1)$$

After the  $(i-1)$ -th collision (at time  $t_{i-1}$ ), the ball makes a projectile motion with gravitational acceleration  $g$ . The position of the ball  $X(t)$  during its flight between two collisions, which take place at time  $t_{i-1}$  and  $t_i$ , is described by the following equation:

$$X(t) = X(t_{i-1}) + v(t_{i-1}) \cdot (t - t_{i-1}) - \frac{1}{2}g \cdot (t - t_{i-1})^2 \quad (2)$$

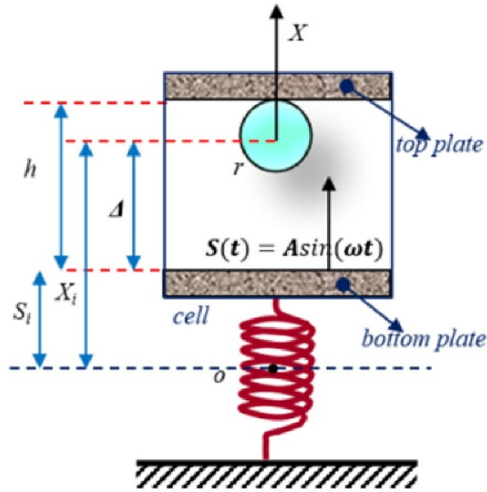


Figure 1. Bouncing ball system of the BB-TENG.

where  $v(t_{i-1})$  is the velocity of the ball at last collision, and it can be described by

$$v(t_{i-1}) = u(t_{i-1}) + \dot{s}(t_{i-1}) \quad (3)$$

where  $u(t_{i-1})$  is the relative velocity between the ball and the cell's bottom plate, when last collision takes place with bottom plate,  $u(t_{i-1}) > 0$  is the sufficient condition for the 'takeoff' of the ball from the cell plate. On the contrary, when last collision takes place with top plate,  $u(t_{i-1}) < 0$ . And collision takes place when the ball and the cell plate are at the same position,  $\Delta(t_i) = r$  or  $\Delta(t_i) = h - r$ , where  $h$  is the height between bottom and top plate,  $r$  is the radius of the ball, and  $\Delta$  is the relative position of the ball over the bottom plate

$$\begin{aligned} \Delta(t) &= X(t) - S(t) \\ &= A \cdot (\sin\omega t_{i-1} - \sin\omega t) \\ &\quad + [u(t_{i-1}) + A\omega\cos\omega t_{i-1}](t - t_{i-1}) \\ &\quad - \frac{1}{2}g \cdot (t - t_{i-1})^2. \end{aligned} \quad (4)$$

The solution  $t_i$  is the next collision time. And the relative 'landing' velocity  $u(t_i)_-$  can be obtained by

$$\begin{aligned} u(t_i)_- &= \dot{\Delta}(t_i) \\ &= A\omega \cdot (\cos\omega t_{i-1} - \cos\omega t_i) + u(t_{i-1}) - g \cdot (t_i - t_{i-1}). \end{aligned} \quad (5)$$

After collision, the ball bouncing back with a relative velocity given by

$$u(t_{i-1}) = -\alpha \cdot u(t_i)_- \quad (6)$$

where  $\alpha$  is the restitution coefficient,  $0 < \alpha < 1$ .

The kinetic parameters and the future of the bouncing ball can be obtained by iterating the above dynamical equations, starting from arbitrary initial conditions. The actual BB-TENG

Table 1. Triboelectric sequence of commonly used materials.

POM 1.3-1.4	(Following the left column)
Knitted wool	Polyester (Dacron)
aluminum	Polyisobutylene
Paper	Polystyrene
Nickel, copper	Polyethylene
Brass, silver	Polypropylene
Polyvinyl alcohol	Polyvinyl chloride
(Continued in right column)	PTFE

system is a 3D model, not a 2D model. In addition to collision, the ball movement forms such as scraping, spinning, tangential flight, chattering, and chaos take place too, due to the complex tensor of elastic properties, surface friction, and the local slope of surface. It is difficult to describe the kinetic property of the ball by restitution coefficient and the 2D motion model. Thus, based on the dynamic equation, the following section further studies the motion characteristics of the BB-TENG system with a 3D finite element model.

## 2.2. Simulation model

As shown in figure 2(a), HSI-TENG have a sandwich structure divided into top and bottom plates and a middle sandwich. The bouncing ball relies on vibration energy to reciprocate between the nest-shells in the sandwich, intermittently contacting the top and bottom plates.

Almost all materials have the effect of triboelectricity. Table 2 lists the triboelectric sequence of commonly used materials. It can be found from the table that the copper electrode plate has electronegativity, and PTFE has strong electronegativity due to its high content of fluorine, which explains why it can be used as a material for BB-TENG to generate electricity. As shown in figure 2(b), the PTFE (polytetrafluoroethylene) bouncing ball has electronegativity, and when it comes in contact with the copper films of the top and bottom plates (electrodes), charge transfer occurs, thereby generating alternating current.

As shown in figures 2(a) and (d) nest-shell of BB-TENG is modeled in ADAMS (Version 2017, MDI, US), which is a 3D modal including the outer shell, rubber pads, and a bouncing ball. The rubber pad and the bouncing ball are both made flexible, while others are of rigid bodies. In the process of flexibility, the bouncing ball is divided into 8921 nodes, and the rubber pad is divided into 2315 nodes. A fixed pair is added between the rubber pad and the upper and lower surfaces of the shell, a translational drive pair is added between the shell and the ground, and the function  $y$  of the drive pair is set as follows (expression form in ADAMS):

$$y = A \times \sin(2 \times \text{pi} \times f \times \text{time}) \quad (7)$$

where, 'A' and 'f' refer to the vibration amplitude and frequency (which will be changed during the experiment) respectively, while 'time' is the time parameter. Then force contact is added between the bouncing ball and the split front

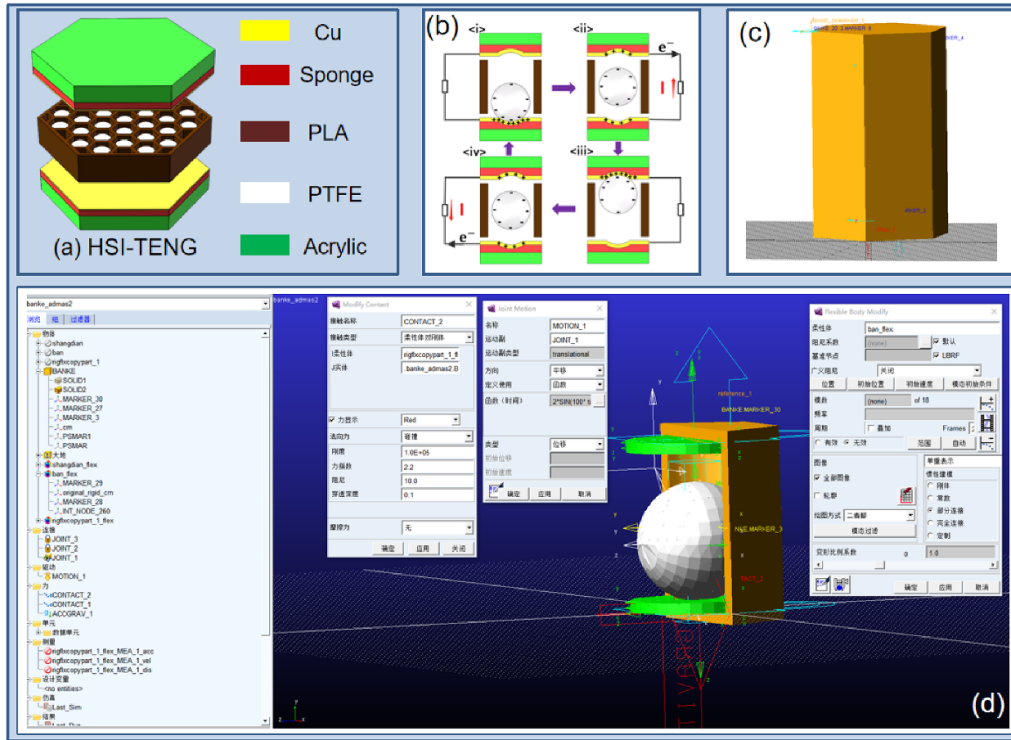


**Figure 2.** Structure, working principle, ADAMS simulation diagram of the BB-TENG. (a) Schematic diagram of HSI-TENG. (b) Schematic diagram of BB-TENG power generation. (c) Simulation diagram of the BB-TENG. (d) Schematic diagram of ADAMS interface.

**Table 2.** Mechanical properties of BB-TENG materials.

Materials	Density/(kg m <sup>-3</sup> )	Modulus of elasticity/MPa	Poisson's ratio
Sponge	500	7.80	0.40
PLA	2200	1140	1.00
PTFE	2300	3140	0.35

and rear plates, and the acceleration of gravity in  $-Y$  direction is increased, the value is  $-9806.65 \text{ mm s}^{-2}$ . The simulation time is set to 2 s, and the number of simulation steps is conventionally 200–300 times the simulation time. In order to ensure the accuracy of the simulation data, the number of steps is set to 1000. The material parameters are set before the start of simulation, as shown in table 2 below.

In order to ensure that the simulation model conforms to the actual structure, the following simplifications and equivalent treatments were made during the modeling process:

- (a) Assume that the vibration form of the bouncing balls in each nest shell is consistent;
- (b) Do not consider the impact of 0.1 mm copper film on model;
- (c) Do not consider the influence of air resistance;
- (d) Do not consider the contact deformation between the excitation table and the BB-TENG's shell.

### 2.3. Simulation model verification

A test with an exciter is conducted to verify the simulation results with the test data. Figure 3(b) is a schematic diagram of the test bench, which consists of JZK-10 modal exciter, SFG-1003 DDS signal generator, YE5871 power amplifier, DLF-8 charge voltage integration filter amplifier, YJ9A7021 acceleration sensor and acquisition oscilloscope equipment. The signal generator provides a harmonically signal for test bench, and modal exciter finally generates a harmonically excitation act on the BB-TENG. The physical test system is shown in figure 3(b). Fix the BB-TENG sample and YJ accelerometer on the plane of the exciter, set the frequency to 30 Hz, adjust the power amplifier knob. BB-TENG sample and YJ accelerometer are connected to the oscilloscope for convenient observation. Figure 3(c) shows the test data, where the maximum acceleration amplitude under this working condition is  $100 \text{ m s}^{-2}$ , and the exciter amplitude calculated by the following formula is 2.8 mm

$$\alpha_{\max} = A(2\pi f)^2. \quad (8)$$

Set the excitation amplitude and frequency as 2.8 mm and 30 Hz in ADAMS. Extract the vertical displacement curve of the bouncing ball from ADAMS, and the result is shown in figure 3(d). It can be found that the vibration frequencies of the bouncing ball under test and simulation are the same, and the trajectories of the bouncing ball under test bench and the simulation are almost the same, so the simulation data can be considered reliable.

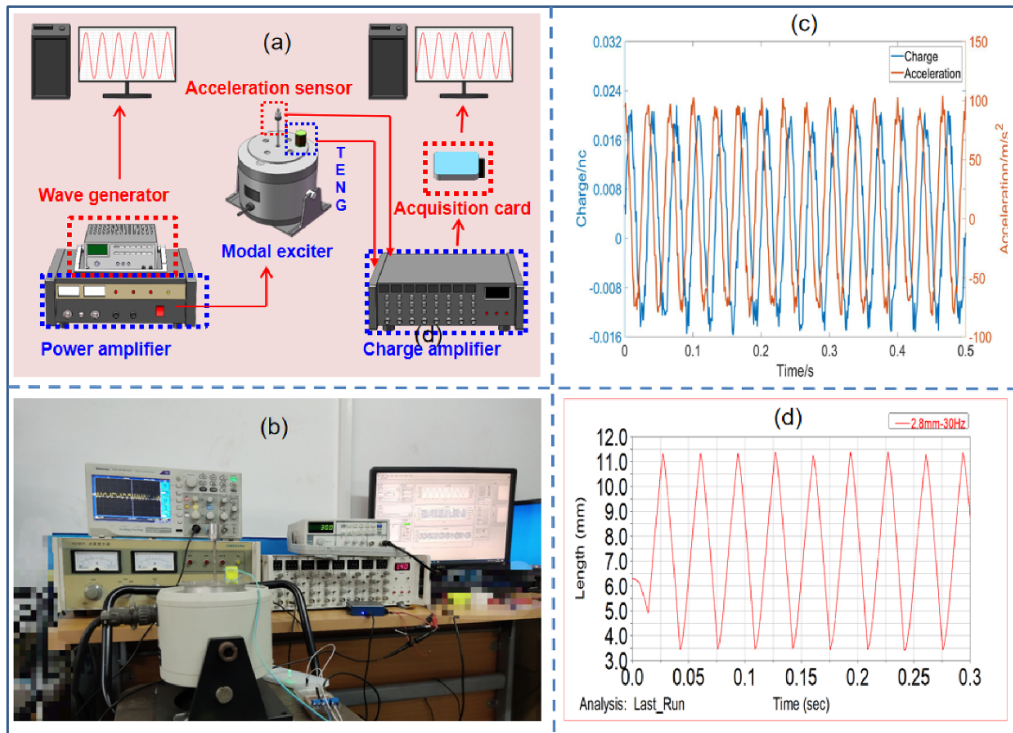


**Figure 3.** Correct setting of the simulation model. (a) Schematic of excitation test. (b) Physical map of excitation test. (c) Diagram of acceleration and charge on bench test. (d) Simulation diagram of the ball’s centroid displacement at 2.8 mm–30 Hz ( $A = 2.8$  mm,  $f = 30$  Hz).

### 3. Results and analysis

Through the simulation of the ADAMS software, we found that the bouncing ball has the following four representative motion characteristics: ‘Take off’, ‘Well-Contact’, ‘Self-Spin’, ‘Rich-Contact’. As shown in figure 4, ‘Take off’ means that the bouncing ball can leave the bottom plate under external excitation. This phenomenon cannot generate a stable AC signal, but it can generate a certain amount of electrical energy on the bottom plate, which is the basis for TENG to convert vibration energy into electrical energy. ‘Well-Contact’ means that the bouncing ball can stably contact the upper plate and generate a relatively stable electrical signal, which is the performance of the stable work of the TENG. ‘Self-Spin’ refers to the phenomenon that the bouncing ball rotates around its own torque when running inside the container; ‘Rich-Contact’ means that the electrical signal generated by the BB-TENG has reached saturation and will not increase with the external excitation.

#### 3.1. ‘Take off’ of the bouncing ball

‘Take off’ refers to the state that the ball becomes separated from the plate and begins to vibrate, which is the premise of BB-TENG’s power generation. The exciter provides a harmonically vibration. As the BB-TENG is fixed on the excitation platform, it can be considered that the motion form of the TENG shell is the same as the excitation platform. The bouncing ball and the shell are in contact through a sponge cushion with stiffness and damping.

The simulation results of ball’s displacement over different excitation frequencies in ADAMS are shown in figure 5(a). It can be found that the displacement curve of the bouncing ball under 10 Hz has a similar amplitude with the exciter, which means the bouncing ball stick on the bottom plate without further movement. When the excitation frequency reaches 12 Hz, the vertical amplitude of the bouncing ball will gradually increase until reaching a peak at 18 Hz.

This indicates that the bouncing ball has a ‘Well-Contact’ with the top plate at 18 Hz. At the same time, it can be found from the position of the bouncing ball during the simulation that the bouncing ball is always close to the bottom plate at 8 Hz and will not ‘Take off’. As the frequency increases, the bouncing ball jumps up and gradually collides with the top plate, which shows that the kinematic relationship of the simulation model is consistent with the actual situation.

#### 3.2. Critical frequency for ‘Well-Contact’

The phenomenon that the bouncing ball can contact the top plate is stipulated to record as ‘Well-Contact’. The prerequisite for BB-TENG’s work is that the bouncing ball is in ‘Well-Contact’ state. The factors that affect the motion of the bouncing ball include the excitation amplitude, frequency, inclination angle, and the stroke of the bouncing ball.

As the figure 5(a) shown, it is worth noting that when the bouncing ball has not yet reach ‘Well-Contact’, its centroid displacement will increase significantly with the slow increase in frequency. However, when it reaches the ‘Well-Contact’

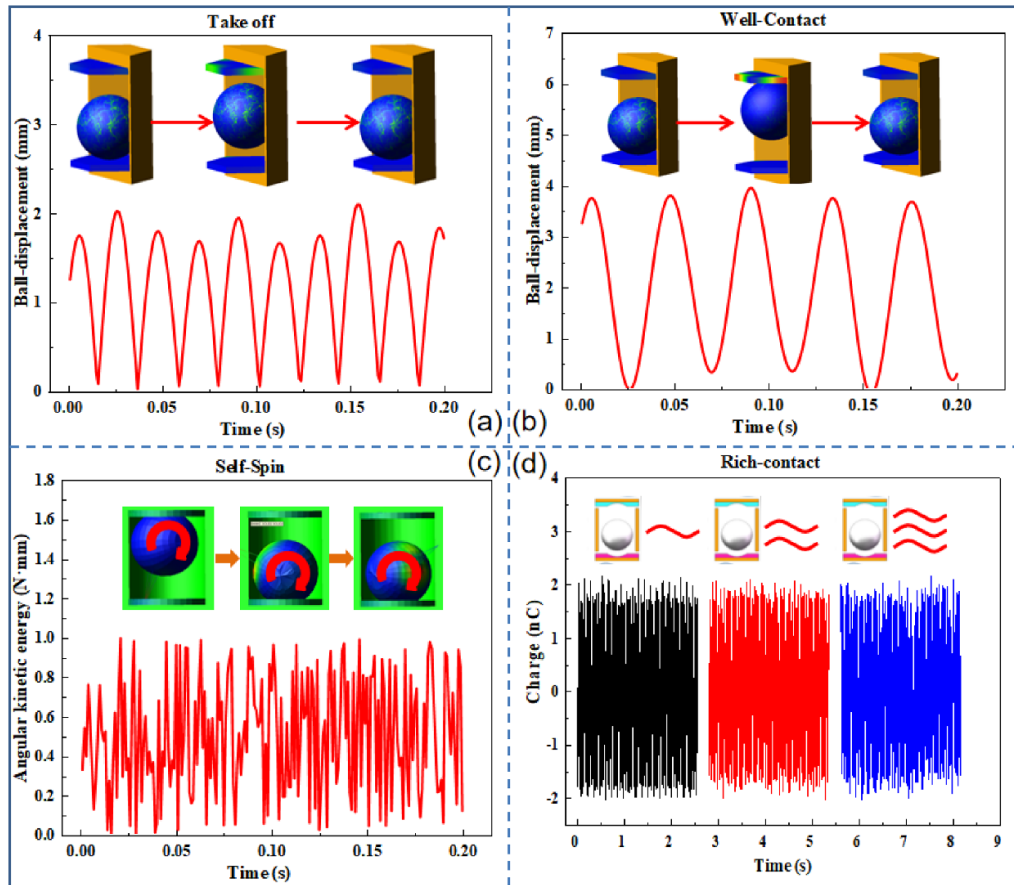


**Figure 4.** The simulation diagrams of the bouncing ball in ADAMS at four states. (a) ‘Take off’. (b) ‘Well-Contact’. (c) ‘Self-Spin’. (d) ‘Rich-Contact’.

state, its amplitude will not have significant changes. For example, the displacement amplitude curves of the bouncing ball at 18 Hz and 20 Hz almost overlap, which is difficult to distinguish. Therefore, we call the frequency at which this phenomenon (e.g. as the frequency increases, the displacement of the ball changes slightly) is critical frequency, and then no more redundant simulation analysis is performed. Based on the above example with an excitation amplitude of 3 mm, the critical frequencies under amplitudes of 0.5, 1, 2 ... 4.5, 5 mm were simulated and calculated to obtain the data.

Interpolating the simulation data to gain the ball-height at particular vibration amplitude and frequency, then the result is shown in figure 5(b). As shown in figures 5(c), (d), it can be found from the Frequency-Height diagram that the bouncing balls will reach the max height when the frequency exceeds 30 Hz at each amplitude, which means that the bouncing balls have ‘Well-Contact’ with the top and bottom plate. The height of the bouncing ball can be easily obtained where it begins to vibrate for each situation from the Amplitude-Height diagram. It also can be obviously found that it is not easy for the bouncing ball to contact with the top and bottom plate when the vibration frequency is lower than 9 Hz. Sorting out the above data, as shown in figure 5(e), when the amplitude is 1 mm, the critical vibration frequency is higher

at about 30 Hz. As the amplitude increases, the critical frequency decreases rapidly. This means that BB-TENG has wide vibration frequency adaptability and difficulty in vibration under small amplitude when harvesting mechanical vibration energy. When the vibration amplitude reaches 3 mm, the critical frequency will have slight changes with the increase of the amplitude, which shows that BB-TENG needs a lowest critical frequency before the bouncing ball of ‘Well-Contact’, and the BB-TENG is difficult to work under the vibration below 9 Hz in the vertical situation. Similarly, as shown in figure 5(f), according to the above steps, the critical frequency at the included angle of 30 degrees can be calculated. It can be found that the required critical frequency of BB-TENG for the same amplitude will decrease as the angle decreases, which is in line with the classic Newton’s Law and proves the universality of the conclusion of the simulation outlined above.

It can be found from figures 6(a) and (b) that in the case of 0.5 mm excitation amplitude, the bouncing ball’s critical frequency needs to reach 100 Hz. Besides, a comparison between figures 5 and 6 shows that when the excitation amplitude of the bouncing ball is greater than 1 mm, the period of its centroid displacement is the same as that of the excitation. When working condition of the ball is 0.5 mm–50 Hz, it can be found that the period of the centroid of the bouncing ball is less than that

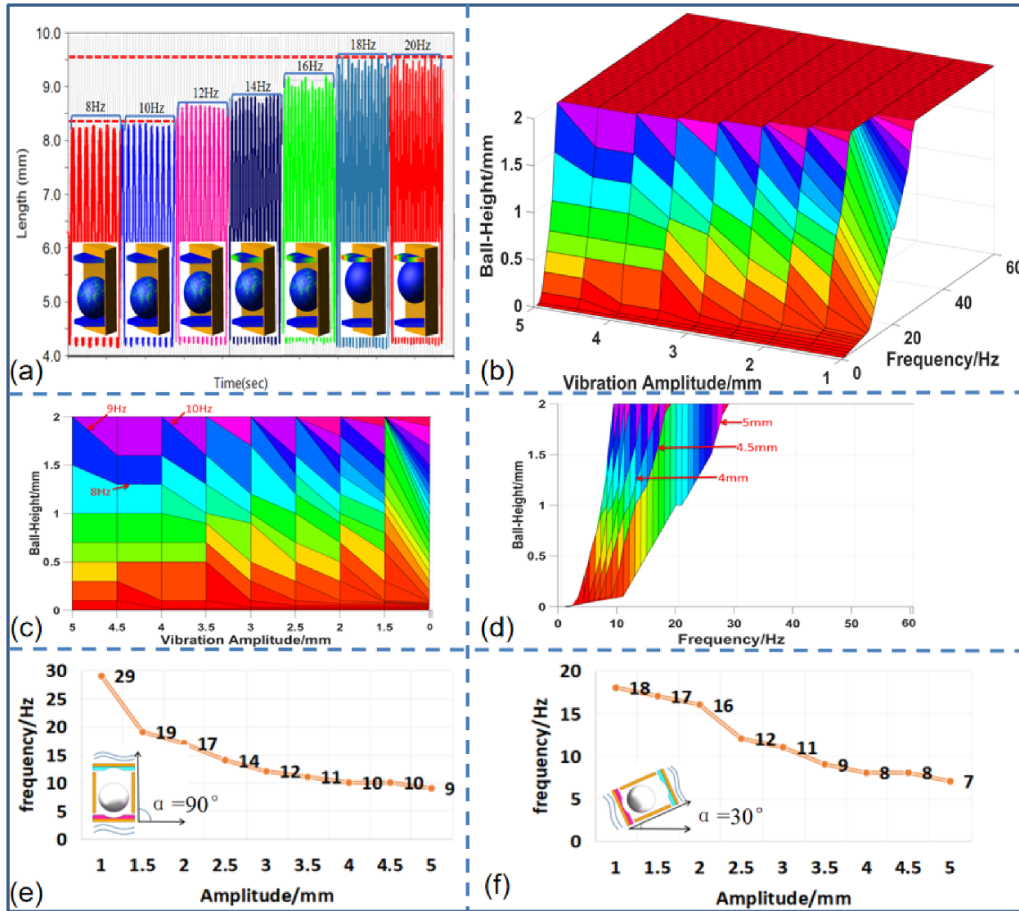


**Figure 5.** Excitation amplitude, excitation frequency, inclination angle will affect ‘Well-Contact’ of bouncing ball (a) bouncing ball’s displacement under excitation amplitude of 3 mm. (b) Three-dimensional diagram of vibration height-frequency-amplitude after interpolation. (c) The vibration height of each amplitude at each frequency. (d) The vibration height of each frequency at each amplitude. (e) ‘Well-Contact’ frequency at each excitation amplitude when vertical. (f) ‘Well-Contact’ frequency at each excitation amplitude when the inclination angle is 30 degrees.

of the excitation frequency (23 crests appear in the centroid displacement of the bouncing ball in 1 s, about 23 Hz). It can also be seen from the simulation that the bouncing ball moves for one cycle and the shell moves for multiple cycles, as shown in figure 6(c). This phenomenon causes a waste of vibration energy and reduces the power generation efficiency.

### 3.3. ‘Self-Spin’ of bouncing ball

As shown in figure 8(a), ‘Self-Spin’ of bouncing ball refers to a phenomenon in which the bouncing ball rotates around its own centroid during vibration. This phenomenon can occur at any stage of the operation of BB-TENG. In order to study the effect of bouncing ball spin on power generation, an experiment is made to simulate the contact between the ball and the electrode plate, as shown in figure 7.

The test is carried out on a spin-speed-controllable ball-plate collision test bench. As shown in figures 7(a)–(c), the test bench includes 42BYGH34 stepper motor, ZMC-200 stepper motor controller, LED display, aluminum alloy flexible coupling, MOFLON conductive ring, copper film, wire, 10 mm diameter PTFE bouncing ball, 25 mm transparent insulating

plastic tube and the charge signal amplification and acquisition device mentioned above. In the test, a motor is used to drive the rotation of the electrode plate to simulate the collision of the bouncing ball with the electrode plate in the case of spinning. The drop height of the bouncing ball is 300 mm, the motor speed range is 0–1200 r min<sup>-1</sup>, divided at 100 r min<sup>-1</sup> intervals (including static working conditions) into 13 different speeds, and the electrical signal at the moment of the bouncing ball landing is measured separately. The collision is performed many times under each working condition to avoid the impact of accidental errors and noise.

Let the bouncing ball contact the stationary plate and the rotating plate in turn, collect the charge transfer signal generated during the collision, it can be found that the latter will increase the amount of charge transfer, and this kind of spin is beneficial. As shown in figure 7(d), through the comparison between 200 r min<sup>-1</sup> and stationary signal, it can be found that when the bouncing ball lands with the motor rotating, the charge signal excited by collision is significantly higher than that with motor at rest.

When the ball is in contact with the shell wall, its spin will also increase frictional consumption and cause energy loss,



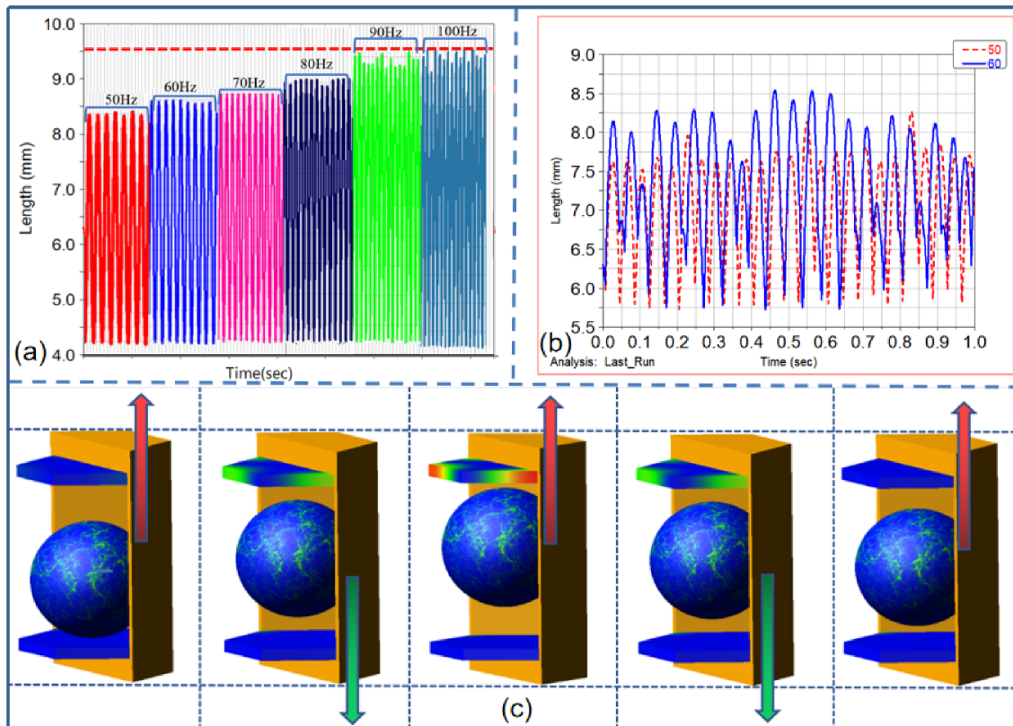


**Figure 6.** ‘Poor-contact’ of the bouncing ball at small excitement amplitude. (a) The ball’s centroid displacement of each frequency at 0.5 mm amplitude. (b) The ball’s centroid displacement at 0.5 mm amplitude, 50 Hz and 60 Hz. (c) The simulation diagram of the bouncing ball at 0.5 mm–50 Hz.

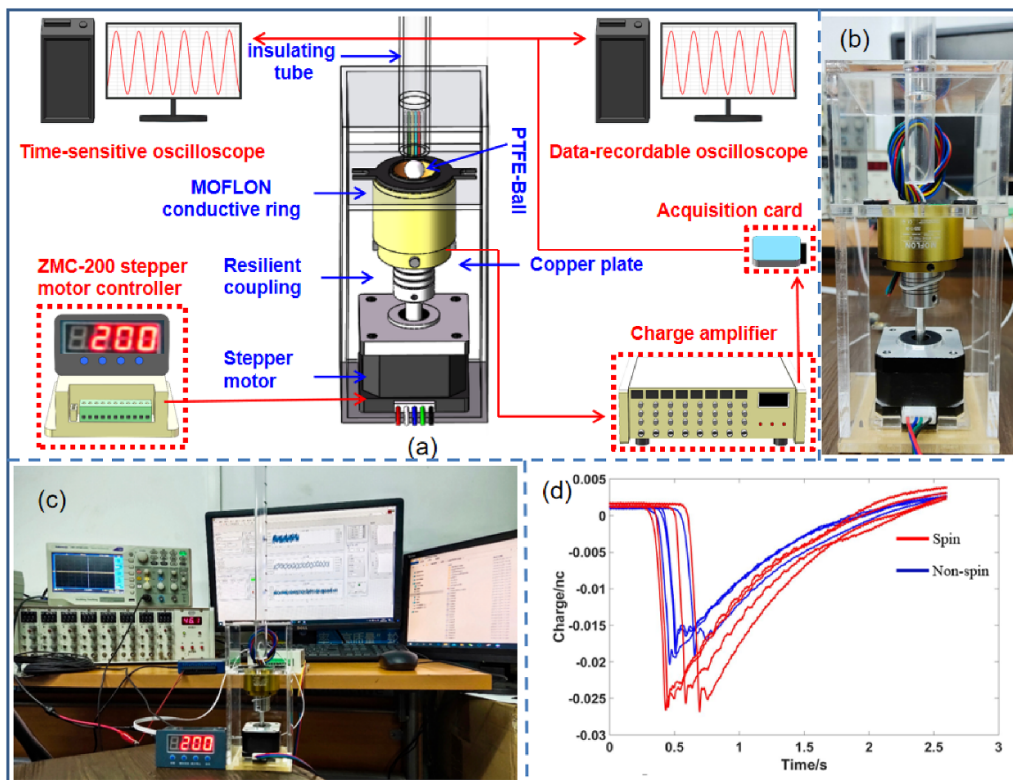


**Figure 7.** The ‘Self-Spin’ of bouncing ball increases the amount of charge transfer. (a) Schematic diagram of spin test. (b) The structure of rotational polar plate. (c) Spin test rig physical model. (d) Spin and non-spin signal diagram.

**Table 3.** Table of amplitude and frequency.

	Amplitude/mm	Frequency/Hz
Small/low	1	20
Medium/medium	3	40
Large/high	5	60

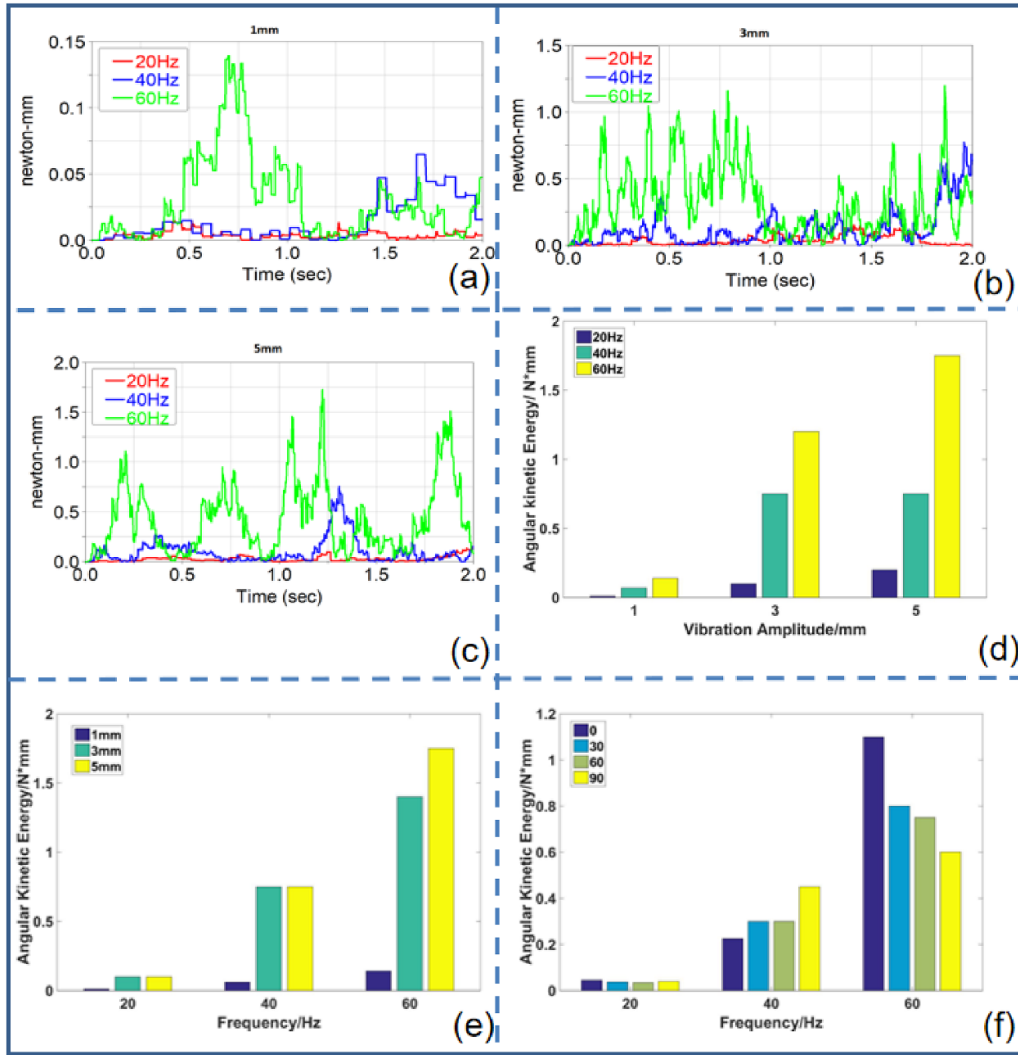


**Figure 8.** ‘Self-Spin’ of the bouncing ball is mainly affected by the excitation frequency. (a)–(c) Figure of angular kinetic energy of each frequency at 1 mm, 3 mm, 5 mm excitation amplitude. (d) The angular kinetic energy is plotted by frequency. (e) The angular kinetic energy is plotted by vibration amplitude. (f) The angular kinetic energy is plotted by inclination angle.

and this kind of spin is harmful. Therefore, the study of bouncing ball spin during vibration is of great significance.

**3.3.1. Coupling effect of exciting amplitude and frequency on spin.** In actual application, the vibration amplitude is generally 1–5 mm, and the frequency is 10–60 Hz. According to table 2, the following divisions are made to facilitate discussion. Some areas belong to the poor contact frequency band, which has been omitted during the division, and no redundant simulation analysis will be performed during the simulation.

Angular kinetic energy  $E_k$  refers to the kinetic energy of an object rotating around an axis, the formula is expressed as

$$E_k = \frac{1}{2} \mathbf{J} \omega^2 \tag{9}$$

where  $\mathbf{J}$  is the inertia of rotation,  $\omega$  is the angular velocity. Therefore, angular kinetic energy can be used to measure the spin intensity of the bouncing ball.

Taking the BB-TENG simulation model with a stroke of 2 mm as an example, according to table 3, the bouncing

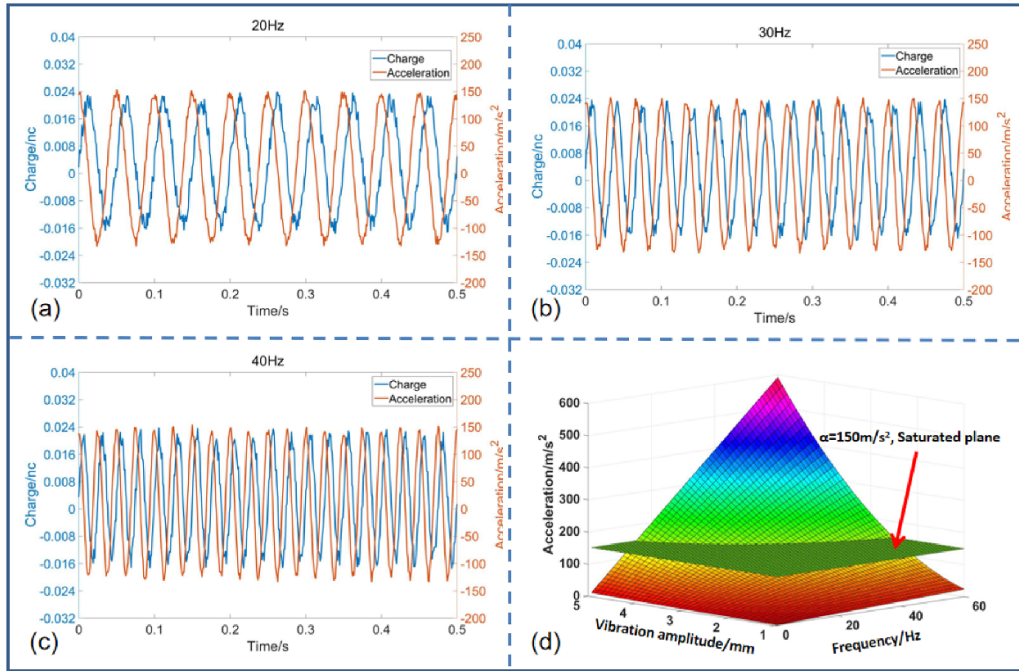


**Figure 9.** There is a certain acceleration to make the BB-TENG charge transfer amount saturated. (a) The diagram of acceleration and charge transfer curve at 20 Hz. (b) The diagram of acceleration and charge transfer curve at 30 Hz. (c) The diagram of acceleration and charge transfer curve at 40 Hz. (d) The diagram of saturated plane.

ball’s angular kinetic energy under various simulation conditions is extracted, and the result is shown in figure 8. From figures 8(a)–(c), it can be found that the angular kinetic energy of the bouncing ball increases rapidly with the increase of its frequency. This situation is especially obvious under the large amplitude (5 mm). Under small amplitude (1 mm) and medium amplitude (3 mm), angular kinetic energy will also increase with the increase of frequency. Under small amplitude, medium frequency and high frequency have little effect on angular kinetic energy.

It can be found from figure 8(d) that the frequency has a significant influence on ‘Self-Spin’. The maximum angular kinetic energy under 20 Hz is about  $0.15 \text{ N} \cdot \text{mm}$ , but that under 40 Hz and 60 Hz is about  $0.8 \text{ N} \cdot \text{mm}$  and  $1.8 \text{ N} \cdot \text{mm}$  respectively, which have an order of magnitude difference. The angular kinetic energy of bouncing ball in low-frequency band (20 Hz) barely changes rapidly. However, in high-frequency band (60 Hz), as shown in figures 8(a)–(c), many ‘steep peaks’ exist in the diagram, which means that bouncing balls have severe collisions during these ‘peaks’. Besides, it can be found from the simulation of the bouncing ball that the angular kinetic energy of the bouncing ball will increase nearly every time when it has a scratch will the shell wall. Therefore, it can be considered that the ‘Self-Spin’ of the bouncing ball is mainly produced by the friction between the bouncing ball and the shell wall. The bouncing ball will gain a torque from the friction to start the ‘Self-Spin’.

**3.3.2. The effect of inclination angle on spin.** Since the frequency has a significant influence on the spin of the bouncing ball, three frequency bands (low, medium, and high) are

selected in sequence, and the medium amplitude of 3 mm is considered to explore the effect of frequency and inclination angle on the spin. The following simulation test is carried out, with the result shown in figure 8(f). Based on the above data, it can be found that when the excitation frequency is low (20 Hz), the angular kinetic energy at each angle is very small. The angle will also have a specific effect on the angular kinetic energy in general but is not the decisive factor, and the angular kinetic energy cannot be significantly increased by changing the angle. In the low and middle frequency bands, the effect of angle is not obvious. In the high frequency band, when the inclination angle is 90 degrees, the angular kinetic energy is the largest and the spin is the strongest. The angular kinetic energy of the BB-TENG will be the highest at an inclination angle of 0 degree and lowest at an inclination angle of 90 degrees, while the values of the maximum kinetic energy are similar when the inclination angle is 30 degrees and 60 degrees, with the maximum value being twice of the minimum one. Therefore, it can be deduced that the inclination angle may exert a significant impact on the ‘Self-Spin’ of the bouncing ball.

**3.4. Saturation analysis for ‘Rich-Contact’**

During the experiment, it was found that the amount of charge transfer of BB-TENG would gradually stabilize in some cases and no longer increase with the increase of excitation frequency and excitation amplitude. The following experiments are carried out to confirm the existence of saturation state of TENG.

The BB-TENG is tested on the excitation test bench, with the excitation frequency set to be 20 Hz, 30 Hz, and 40 Hz (it is

difficult to start vibration below 20 Hz). The power amplifier is adjusted continuously to gradually increase the excitation vibration acceleration until the amount of transferred charge no longer increases, and the measured acceleration and charge transfer amount at each frequency are shown in figure 9.

It can be found that the maximum amount of charge transfer at each frequency is 0.023nC, and the YJ accelerometer reading is  $150 \text{ m s}^{-2}$ . It can be considered that the amount of charge transfer has reached saturation at this acceleration, and it is not very meaningful to increase the excitation energy, but increasing the frequency will increase the rate of charge transfer, which in turn increases the current. According to the formula [5], and the above conclusions, a vibration amplitude-frequency-acceleration diagram is plotted with a saturated acceleration plane of  $150 \text{ m s}^{-2}$ , as shown in figure 9(d). The working conditions (amplitude, frequency) corresponding to acceleration above the plane are all in saturation, which should be avoided as much as possible to improve energy utilization.

#### 4. Conclusions

This work has successfully studied the kinetic and electrical performance of the bouncing ball in BB-TENG, which is usually used to harvest vibrational energy and sense signal for self-powered smart sensor. The energy harvesting efficiency and sensing effectiveness are significantly affected by the kinetic performance of the bouncing ball. Exploration was also made on the four states of the bouncing ball during its collision with plate electrodes and flight between plates, namely the 'Takeoff', 'Well-Contact', 'Self-Spin' and 'Rich-Contact' states.

At the 'Takeoff' state, BB-TENG's vibration energy starts to be converted into electrical energy, the 'well-contact' state is the basis for its stable current generation, the 'Self-Spin' state generated by the unbalanced excitation torque will increase energy harvesting and the 'Rich-Contact' state leads to a waste of energy. External vibration conditions have more significant influence on these four states. Although we may not be able to change the external vibration conditions, we can use the simulation analysis method to quickly optimize the BB-TENG structure and bouncing ball size, making the BB-TENG quickly adapt to the working conditions and run in the 'Well-Contact' and 'Self-Spin' states as much as possible, so as to avoid unnecessary energy waste.

#### Data availability statement

All data that support the findings of this study are included within the article (and any supplementary files).

#### Acknowledgments



Acknowledgements are addressed to the joint support from the National Natural Science Foundation of China (Grant Nos. 51879022, 51979045, 51906029), the Fundamental

Research Funds for the Central Universities, China (Grant No. 3132019330), and Projects for Dalian Youth Star of Science and Technology (Grant No. 2018RQ12).

#### Conflict of Interest

The authors declare no conflict of interest.

#### ORCID iDs

Chaoming Huang  <https://orcid.org/0000-0003-4132-1233>  
Minyi Xu  <https://orcid.org/0000-0002-3772-8340>

#### References

- [1] Chen H T, Song Y, Cheng X L and Zhang H X 2019 Self-powered electronic skin based on the triboelectric generator *Nano Energy* **56** 252–68
- [2] Chen J and Wang Z L 2017 Reviving vibration energy harvesting and self-powered sensing by a triboelectric nanogenerator *Joule* **1** 480–521
- [3] Cheng P *et al* 2019 Largely enhanced triboelectric nanogenerator for efficient harvesting of water wave energy by soft contacted structure *Nano Energy* **57** 432–9
- [4] Ding W B, Wang A C, Wu C S, Guo H Y and Wang Z L 2019 Human-machine interfacing enabled by triboelectric nanogenerators and tribotronics *Adv. Mater. Technol.* **4** 1800487
- [5] Dong K, Wang Y C, Deng J N, Dai Y J, Zhang S L, Zou H Y, Gu B, Sun B and Wang Z L 2017 A highly stretchable and washable all-yarn-based self-charging knitting power textile composed of fiber triboelectric nanogenerators and supercapacitors *ACS Nano* **11** 9490–9
- [6] Guo H Y *et al* 2018 A highly sensitive, self-powered triboelectric auditory sensor for social robotics and hearing aids *Sci. Robot.* **3** eaat2516
- [7] Xiao X *et al* 2019 Honeycomb structure inspired triboelectric nanogenerator for highly effective vibration energy harvesting and self-powered engine condition monitoring *Adv. Energy Mater.* **9** 1902460
- [8] Pang Y K, Chen S E, Chu Y H, Wang Z L and Cao C Y 2019 Matryoshka-inspired hierarchically structured triboelectric nanogenerators for wave energy harvesting *Nano Energy* **66** 104131
- [9] Chen J, Chen B, Han K, Tang W, Wang Z L and Triboelectric A 2019 Nanogenerator as a self-powered sensor for a soft-rigid hybrid actuator *Adv. Mater. Technol.* **4** 1900337
- [10] Wang Z L 2013 Triboelectric nanogenerators as new energy technology for self-powered systems and as active mechanical and chemical sensors *ACS Nano* **7** 9533–57
- [11] Perutz M F, Fermi G, Poyart C, Pagnier J and Kister J 1993 A novel allosteric mechanism in haemoglobin. Structure of bovine deoxyhaemoglobin, absence of specific chloride-binding sites and origin of the chloride-linked Bohr effect in bovine and human haemoglobin *J. Mol. Biol.* **233** 536–45
- [12] Luck J M, Mehta A 1993 Bouncing ball with a finite restitution: chattering, locking, and chaos *Phys. Rev. E* **48** 3988–97
- [13] Garcia C and Trendafilova I 2019 Real-time diagnosis of small energy impacts using a triboelectric nanosensor *Sens. Actuators A* **291** 196–203

- [14] Garcia C, Trendafilova I, De Villoria R G and Del Rio J S 2018 Self-powered pressure sensor based on the triboelectric effect and its analysis using dynamic mechanical analysis *Nano Energy* **50** 401–9
- [15] Garcia C, Trendafilova I, Guzman De Villoria R and Sanchez Del Rio J 2018 Triboelectric nanogenerator as self-powered impact sensor *Int. Conf. on Engineering Vibration. MATEC Web of Confs.* ed E Manoach, S Stoykov and M Wiercigroch p 148
- [16] Han J, Li H and Fu T 2021 A pulsed freestanding triboelectric nanogenerator and power management circuit to harvest rotation energy from an automobile brake *J. Micromech. Microeng.* **31** 015007
- [17] He T Y Y, Sun Z D, Shi Q F, Zhu M L, Anaya D V, Xu M Y, Chen T, Yuce M R, Thean A V-Y and Lee C 2019 Self-powered glove-based intuitive interface for diversified control applications in real/cyber space *Nano Energy* **58** 641–51
- [18] Jiang C M, Wu C, Li X J, Yao Y, Lan L Y, Zhao F N, Ye Z, Ying Y and Ping J 2019 All-electrospun flexible triboelectric nanogenerator based on metallic MXene nanosheets *Nano Energy* **59** 268–76
- [19] Kwak S S, Yoon H J and Kim S W 2019 Textile-based triboelectric nanogenerators for self-powered wearable electronics *Adv. Funct. Mater.* **29** 1804533
- [20] Lai Y C, Deng J, Zhang S L, Niu S, Guo H and Wang Z L 2017 Single-thread-based wearable and highly stretchable triboelectric nanogenerators and their applications in cloth-based self-powered human-interactive and biomedical sensing *Adv. Funct. Mater.* **27** 1604462
- [21] Li M N, Porter A L and Wang Z L 2017 Evolutionary trend analysis of nanogenerator research based on a novel perspective of phased bibliographic coupling *Nano Energy* **34** 93–102
- [22] Lin Z M, Chen J, Li X S, Zhou Z H, Meng K Y, Wei W, Yang J and Wang Z L 2017 Triboelectric nanogenerator enabled body sensor network for self-powered human heart-rate monitoring *ACS Nano* **11** 8830–7
- [23] An H, Chen L, Liu X, Wang X, Liu Y, Wu Z, Zhao B and Zhang H 2021 High-sensitivity liquid-metal-based contact lens sensor for continuous intraocular pressure monitoring *J. Micromech. Microeng.* **31** 035006
- [24] Brace E, Ghaderian S, Ghannoum A and Nieva P 2021 Impact of support material deformation in MEMS bulk micromachined diaphragm pressure sensors *J. Micromech. Microeng.* **31** 055001
- [25] Dong H, Le X, Pang K, Pang J, Li D, Xu Z, Gao C and Xie J 2021 A serial flexible humidity sensor based on graphene oxide fibers and quartz crystal resonator *J. Micromech. Microeng.* **31** 025004
- [26] Han X *et al* 2021 High-accuracy differential resonant pressure sensor with linear fitting method *J. Micromech. Microeng.* **31** 045006
- [27] Karlsson A, Bergman H and Johansson S 2021 Active real-time electric field control of the e-jet in near-field electrospinning using an auxiliary electrode *J. Micromech. Microeng.* **31** 035001
- [28] Lin Y C, Cai M X and Yang Y J 2021 A wireless passive pressure sensor using microstructured ferromagnetic films with tunable effective permeability *J. Micromech. Microeng.* **31** 045017
- [29] Liu L, Ji W, Xing Z, Sun X, Chen Y, Du Y and Qin F 2021 A dual-frequency piezoelectric micromachined ultrasound transducer array with low inter-element coupling effects *J. Micromech. Microeng.* **31** 045005
- [30] Liu W, Chen Z, Kan X, Wang T, Jia Q, Zhu Y, Zhao J, Yuan Q, Yang J and Yang F 2021 Novel narrowband radio frequency microelectromechanical systems filters *J. Micromech. Microeng.* **31** 025003
- [31] Pallay M, Daeichin M and Towfighian S 2021 Feasibility study of a micro-electro-mechanical-systems threshold-pressure sensor based on parametric resonance: experimental and theoretical investigations *J. Micromech. Microeng.* **31** 025002
- [32] Shi Y, Lu K, Li B, Chen Y, Xi X, Wu Y, Wu X and Xiao D 2021 Ultrafast laser in fabrication of micro hemispherical resonators with quality factor over millions *J. Micromech. Microeng.* **31** 055002
- [33] Barroso J J, Carneiro M V and Macau E E N 2009 Bouncing ball problem: stability of the periodic modes *Phys. Rev. E* **79** 026206
- [34] Smith N D, Swift M R and Smith M I 2021 Collision-enhanced friction of a bouncing ball on a rough vibrating surface *Sci. Rep.* **11** 442
- [35] Zhang B *et al* 2017 Self-powered acceleration sensor based on liquid metal triboelectric nanogenerator for vibration monitoring *ACS Nano* **11** 7440–6
- [36] Xu M, Wang P, Wang Y-C, Zhang S L, Wang A C, Zhang C, Wang Z, Pan X and Wang Z L 2018 A soft and robust spring based triboelectric nanogenerator for harvesting arbitrary directional vibration energy and self-powered vibration sensing *Adv. Energy Mater.* **8** 1702432